Drug Design, Development and Therapy

Dovepress
Taylor & Francis Group

Open Access Full Text Article

ORIGINAL RESEARCH

Sevoflurane Alleviates Cardiomyocyte Ferroptosis via Ubiquitin-Specific Protease 7/Phosphatase and Tensin Homolog Modulation

Jiashun Xu[1]*, Zongyue Wang[1]*, Huifang Wei[1]*, Liqin Wang[1], Yun Hong[1], Wenqing Xu[2], Meifen Ding[1], Zheming Song[1]

[1]Department of Anesthesiology, No. 905 Hospital of People's Liberation Army Navy, Shanghai, 200050, People's Republic of China; [2]Department of Respiratory and Critical Care Medicine, Shanghai Changzheng Hospital, Shanghai, 200003, People's Republic of China

*These authors contributed equally to this work

Correspondence: Zheming Song, Department of Anesthesiology, No. 905 Hospital of People's Liberation Army Navy, No. 1328 Huashan Road, Changning District, Shanghai, 200050, People's Republic of China, Email nav905hospitalmzk@163.com

Background and Objective: Myocardial ischemia-reperfusion (I/R) injury remains a significant challenge in the treatment of acute myocardial infarction, highlighting the urgent need for effective cardioprotective strategies. Sevoflurane (Sev), a widely used anesthetic, has demonstrated notable cardioprotective potential. This study investigated whether Sev mitigates ferroptosis in myocardial cells by inhibiting the USP7-mediated PTEN/PI3K/AKT pathway.

Methods: Rat myocardial I/R injury and H9c2 cell hypoxia/reoxygenation (H/R) injury models were established. Myocardial injury was assessed through cTnT levels, hemodynamic parameters, and histological analyses. Cell viability, LDH release, TUNEL staining, and ferroptosis markers (GSH, MDA, Fe^{2+}, ROS) were evaluated. Co-IP and CHX assays were employed to explore USP7's regulation of PTEN stability.

Results: Sev significantly reduced serum cTnT levels, improved hemodynamic function, decreased infarct size, and alleviated myocardial fibrosis and inflammation in rats subjected to I/R injury. In H9c2 cells, Sev enhanced cell viability and suppressed apoptosis. Sev reversed hypoxia/reoxygenation (H/R)-induced USP7 overexpression and ferroptosis, whereas USP7 overexpression attenuated Sev's protective effects.

Conclusion: Sev protected against myocardial I/R injury by inhibiting USP7, destabilizing PTEN, activating the PI3K/AKT pathway, and suppressing ferroptosis. These findings elucidated the molecular mechanism of Sev's cardioprotective effect and suggested USP7 as a potential therapeutic target for myocardial protection.

Keywords: sevoflurane, USP7, ferroptosis, ischemia, PTEN

Introduction

Myocardial ischemia-reperfusion (I/R) injury refers to tissue damage caused by the recovery of blood flow in the myocardium after experiencing an ischemic state, and is a common complication in the treatment of acute myocardial infarction.[1,2] The existing clinical treatment methods mainly include drug therapy and interventional surgery.[3] Although they can reduce damage to a certain extent, they cannot completely prevent the death of myocardial cells.[4] Recent studies have identified ferroptosis, a regulated form of iron-dependent cell death characterized by lipid peroxidation and reactive oxygen species accumulation, as an important contributor to myocardial I/R injury.[5,6] Ferroptosis aggravates myocardial cell loss and exacerbates cardiac dysfunction, highlighting the need to better understand its regulatory mechanisms.[7] Therefore, exploring new protective strategies and mechanisms to alleviate the damage of myocardial I/R injury, particularly by targeting ferroptosis, is particularly important.

In recent years, sevoflurane (Sev), as a commonly used volatile anesthetic, has the advantages of fast onset, stable metabolism, and rapid recovery, making it one of the preferred drugs in general anesthesia.[8] In addition to its wide application

Received: 28 March 2025
Accepted: 16 July 2025
Published: 23 July 2025

in the field of anesthesia, its significant cardioprotective potential has also received attention.[9,10] Research has shown that Sev has the potential to alleviate myocardial I/R injury,[11] particularly in reducing oxidative stress response and regulating cell death.[12] Although the cardioprotective effect of Sev has been validated in multiple experimental models, its specific molecular mechanism is still unclear. Therefore, finding its targets and elucidating its protective mechanism has become a current research focus.

Ubiquitin-Specific Protease 7 (USP7), a pivotal deubiquitinase, plays a crucial role in regulating protein stability and function by removing ubiquitin chains from target proteins.[13] In recent years, many studies have confirmed that USP7 not only participates in regulating cell proliferation, apoptosis, and DNA damage repair,[14] but is also closely related to various pathological processes, especially its role in ferroptosis has gradually been revealed.[15,16] Iron dependent cell death is a novel cell death mechanism that relies on iron ions and lipid peroxidation.[17] Studies have found that USP7 can affect the progression of iron dependent cell death by regulating the ubiquitination status of its substrate proteins.[18] Moreover, increasing evidence indicates that USP7 is involved in the development of cardiovascular diseases, where it regulates oxidative stress and inflammatory responses-key pathogenic factors in myocardial I/R injury.[19] USP7-mediated deubiquitination has been found to modulate signaling pathways related to reactive oxygen species (ROS) production and antioxidant defenses, thereby affecting cardiomyocyte survival under stress conditions.[20] These findings suggest that USP7 plays a crucial role in cardiac pathophysiology by linking ubiquitin-mediated regulation with oxidative stress and ferroptosis.

Phosphatase and Tensin Homolog (PTEN), a well-established tumor suppressor, is recognized as a key regulator of cell survival and proliferation. Its function is intricately linked to the process of ferroptosis.[21] Moreover, the deubiquitination modification of PTEN can affect its stability, thereby affecting the cell's response to oxidative stress.[22] In addition, the function of PTEN is mainly achieved by regulating the PI3K/AKT signaling pathway.[23] In the context of myocardial I/R injury, the PI3K/AKT signaling pathway is considered an important protective pathway,[24] which can promote myocardial cell survival and inhibit various forms of cell death, including ferroptosis.[25] Therefore, USP7, by regulating the activity and stability of PTEN, will help activate the PI3K/AKT signaling pathway, thereby reducing myocardial cell damage. This will provide a new perspective on the pharmacological mechanism of Sev.

Based on the above background, we reasonably assume that Sev may alleviate iron death in cardiomyocytes by inhibiting the expression of USP7, reducing the stability of PTEN, and releasing its negative regulation of the PI3K/AKT signaling pathway. Further research will validate this hypothesis and elucidate the molecular protective mechanism of Sev in myocardial I/R injury, providing new targets for clinical intervention.

Methods

Animal Modeling

Seventy male Sprague-Dawley (SD) rats aged 10 weeks and weighing 368–411 g were purchased from Vital River Laboratory Animal Technology Co., Ltd. (Beijing, China). The feeding environment for all rats was as follows: room temperature at 25 ± 5°C, humidity of 60 ± 5%, free access to food and drinking water, constant light: dark (12: 12 hours) cycle, and adaptive feeding for 7 days prior to experimentation. Male SD rats were randomly divided into seven groups (n = 10/group): Sham, Model, Sev, Sev + oe-NC, Sev + oe-USP7, Sev + oe-USP7 + sh-NC, and Sev + oe-USP7 + sh-PTEN. After anesthesia with 2% isoflurane, the rats were placed supine on a heating pad at 37°C. During the experiment, standard limb lead II electrocardiogram monitoring was continuously conducted. Following tracheotomy, a endotracheal tube was inserted and connected to a mechanical ventilator for ventilation. To induce I/R injury, after left chest incision, the left anterior descending coronary artery (LAD) was ligated 2 mm distal to the left atrial appendage-arterial cone junction using a 6–0 suture.[26] At 30-minute post-ischemia, the slipknot was released for reperfusion for 2 hours. Sev at 1.0 minimum alveolar concentration (MAC) (Y0001993, Sigma-Aldrich, St. Louis, USA) was administered via vaporizer during initial 15 minutes of reperfusion, followed by 105 minutes of medical air ventilation.[27] All experimental groups underwent LAD occlusion and reperfusion except for the Sham group. The Sham group received the same thoracotomy procedure but without coronary artery ligation. Consistent with the study design, neither the Sham nor Model groups were exposed to Sev during reperfusion. Two weeks pre-modeling, rats were injected with adeno-associated virus (AAV) constructs encoding oe-NC, oe-USP7, sh-NC, and sh-PTEN via tail vein at a dose of 1×10^{11} v.g per rat.[28] After 2-hour reperfusion, rats were euthanized by intraperitoneal injection of

150 mg/kg pentobarbital sodium, and their myocardial tissues were taken for subsequent experiments. All animal procedures, including group allocation, intervention administration, and outcome assessment, were performed in a blinded manner to minimize experimental bias. All animal experiments were approved by the Animal Ethics Committee of Hunan Evidence-based Biotechnology Co., Ltd. and were conducted in strict accordance with the Guide for the Care and Use of Laboratory Animals (8th edition, 2011) issued by the US National Institutes of Health, to ensure the welfare of laboratory animals and compliance with ethical standards.

Hemodynamic Monitoring

To comprehensively assess cardiac function, a polyethylene catheter was surgically inserted into the left ventricle to record left ventricular hemodynamic parameters, including heart rate (HR), left ventricular systolic pressure (LVSP), left ventricular end-diastolic pressure (LVEDP), maximum rate of left ventricular pressure rise ($+dp/dt_{max}$), and maximum rate of left ventricular pressure decline ($-dp/dt_{max}$), using the RM6240BD multi-channel physiological signal acquisition system (Chengdu Instrument Factory, China). Six predefined time points were established for data acquisition: T1 (20 minutes), T2 (50 minutes), T3 (60 minutes), T4 (120 minutes), T5 (140 minutes), and T6 (150 minutes). In addition, three functional parameters were calculated: left ventricular development pressure (LVDP = LVSP - LVEDP), shock index (SI = HR/LVDP), and rate-pressure product (RPP = HR × LVDP/1000).

Cell Culture and Processing

H9c2 rat cardiomyocytes (R3-0101, Oricellbio, Guangzhou, China) were cultured in DMEM containing 10% fetal bovine serum (HY-T1000, MedChemExpress, New Jersey, USA) under an environment of 37°C, 95% humidity, and 5% CO_2. Hypoxia was induced by placing H9c2 cells in a hypoxia chamber with 1% O_2, 5% CO_2, and 94% N_2 for 3 hours, followed by reoxygenation under normoxic conditions for 6 hours. At reoxygenation onset, cells were exposed to 2% Sev for 15 minutes using a Sev vaporizer within a sealed hypoxia chamber at 37°C, with 2% Sev and O_2 allowed to flow through. According to the instructions of Lipofectamine 3000 transfection reagent (Shanghai GenePharma Co., Ltd., Shanghai, China), the oe-NC, oe-USP7, sh-NC, and sh-PTEN plasmids were transfected into H9c2 cells 24 hours prior to hypoxia-reoxygenation (H/R) induction.[29] All experimental procedures, including group assignment and data collection, were performed in a blinded manner to minimize bias.

Cardiac Troponin T (cTnT) Assay

Rat blood samples were allowed to clot at room temperature for 30 minutes and then centrifuged at 12,000 rpm for 10 minutes at 4 °C using a high-speed refrigerated centrifuge. The supernatant (serum) was collected and stored at −80 °C. cTnT levels were measured using a rat-specific ELISA kit (D731035, Sangon Biotech, Shanghai, China) according to the manufacturer's protocol. Absorbance was read at 450 nm using a microplate reader.

2,3,5-Triphenyl-2H-Tetrazolium Chloride (TTC) Assay

Myocardial tissue samples were rapidly frozen at −20°C for about 20 minutes to optimize slicing consistency, and cut coronally into 5 consecutive sections. Subsequently, sections were incubated in a 2% TTC solution (298–96-4, Yeasen, Shanghai, China) for 20 minutes at 37°C in the dark. Following TTC staining, the slices were fixed in 4% paraformaldehyde (MA0192, Meilune, Dalian, China) for 24 hours and then photographed for recording. Image analysis was performed using ImageJ (V1.8.0.112, NIH, Madison, WI, USA).

Hematoxylin-Eosin (HE) Staining

The collected myocardial tissue samples were fixed, paraffin-embedded, and cut into 3-μm-thick sections. Next, the slices were deparaffinized in xylene I and II (Sigma) for 20 minutes, followed by dehydration using gradient ethanol for 5 minutes each. After washing with distilled water, the slices were stained with hematoxylin for 10 minutes, rinsed with running water, and then counterstained with eosin for 30 seconds. After washing the red dye with distilled water, the slices were dehydrated by gradient ethanol, treated with xylene for transparency, and sealed with neutral resin. Cell

morphology was observed under an optical microscope (CX43, Olympus, Tokyo, Japan) to evaluate the pathological changes in rat myocardium.

Masson's Trichrome Staining

Myocardial tissue sections were firstly stained with 50 μL hematoxylin staining solution for 5 minutes. After removing the staining solution and washing with distilled water for 5 minutes, the sections were differentiated with acidic differentiation solution for 30 seconds, and blued with tap water for 10 minutes. Then, the sections were counterstained with 50 μL Li Chunhong acid fuchsin staining solution for 10 minutes. Following removal of the staining solution, the sections were quickly rinsed with distilled water and differentiated with phosphomolybdic acid for 2 minutes. Next, the sections were added with 50 μL bright green staining solution dropwise for 1 minute, followed by rinsing with distilled water and differentiation with acidic differentiation solution for 1 minute. Finally, the slices were sequentially dehydrated in 70%, 80%, 90%, and anhydrous ethanol for 10 seconds each, and cleared in xylene three times, each time for 1–2 minutes. After sealing, collagen deposition was observed under an optical microscope (CX43, Olympus, Tokyo, Japan) to evaluate the degree of myocardial fibrosis.

Quantitative Reverse Transcription-Polymerase Chain Reaction (RT-qPCR)

Total RNA was extracted from myocardial tissues and H9c2 cells in each experimental group using a rapid RNA extraction kit (DP419, Jiachu Biotechnology Co., Ltd., Shanghai, China) according to the manufacturer's instructions. The concentration and purity of RNA were assessed using a NanoDrop 2000 spectrophotometer (Thermo Fisher Scientific, USA) by measuring absorbance ratios at 260/280 nm and 260/230 nm. RNA integrity was confirmed by electrophoresis on 1% agarose gels. Reverse transcription was performed using a reverse transcription kit following the manufacturer's protocol. Briefly, 1 μg of total RNA was reverse transcribed to cDNA in a 20 μL reaction volume at 37 °C for 15 minutes, followed by inactivation at 85 °C for 5 seconds. Quantitative PCR amplification was performed using a fluorescence quantification PCR kit (QR0100, Sigma-Aldrich, St. Louis, USA) on a real-time PCR system. The cycling conditions were as follows: initial denaturation at 95 °C for 3 minutes, followed by 40 cycles of 95 °C for 15 seconds and 60 °C for 30 seconds. GAPDH was used as an internal reference gene, and relative mRNA expression levels were calculated using the $2^{-\Delta\Delta Ct}$ method. Primer sequences are listed in Table 1.

Immunohistochemistry (IHC)

Myocardial tissue slices were floated in water at 40°C to avoid air bubbles affecting the tissues, followed by sequential dewaxing with xylene and rehydration through ethanol. After rinsing with clean water for a period of time, the slices were soaked in 3% H_2O_2 for 10 minutes to quench endogenous peroxidase activity. Following pouring out H_2O_2, the slices were washed twice with clean water, added with citric acid buffer solution, and heated in a microwave for 3 minutes. After cooling to room temperature, the slices were heated again and re-cooled to room temperature to ensure that the antigen sites were fully exposed. After antigen retrieval, the slices were blocked and incubated overnight with

Table 1 The Sequences of the Primers Used in qPCR Assay

Gene	Direction	Sequence (5'-3')
USP7	F	CCGAGGACATGGAGATGGAAG
	R	AGCCGACATAGCCAGTATGC
GPX4	F	ATTCCCGAGCCTTTCAACCC
	R	TATCGGGCATGCAGATCGAC
FTH1	F	AACTACCACCAGGACTCGGA
	R	GAAGATTCGTCCACCTCGCT
PTEN	F	TCCAATGTTCAGTGGCGGAA
	R	ACCTTTAGCTGGCAGACCAC
GAPDH	F	TGATGGGTGTGAACCACGAG
	R	ATTCGAGAGAAGGGAGGGCT

primary anti-USP7 antibody (1:100, PA5-34911, Thermo Fisher Scientific, MA, USA) at 4°C. After washing, re-incubation was conducted with horseradish peroxidase (HRP)-labeled goat anti-rabbit secondary antibody (1:2000, ab205718, Abcam, Cambridge, UK) for 1 hour. Subsequently, diaminobenzidine (DAB) working solution (P0203, Beyotime, Shanghai, China) was applied for color development, hematoxylin was used for counterstaining, and the staining results were observed using an optical microscope (CX43, Olympus, TKY, Japan). Cells were counted using ImageJ software (DAB-positive area/total myocardial area × 100% = relative positive area).

Western Blot (WB)

Total protein was extracted from myocardial tissues and H9c2 cells using RIPA lysis buffer (ab170197, Abcam, Cambridge, UK). A bicinchoninic acid (BCA) protein assay kit (P0010, Beyotime, Shanghai, China) was used to determine the total protein content. Protein samples of the same amount were separated by sodium dodecyl sulfate-polyacrylamide gel electrophoresis (SDS-PAGE) and electrophoretically transferred onto polyvinylidene fluoride (PVDF) membranes (ab133411, Abcam, Cambridge, UK) using wet transfer method. The membranes were sealed with 5% skim milk powder for 1 hour, and then incubated overnight at 4°C with the following primary antibodies: anti-USP7 (1:1000, PA5-34911, Thermo Fisher Scientific, MA, USA), anti-GPX4 (1:1000, ab125066, Abcam, Cambridge), anti-FTH1 (1:1000, A19544, Abclonal, Wuhan, China), anti-PTEN (1:500, SAB4502474, Sigma-Aldrich, St. Louis, USA), anti-PI3K (1:500, A19742, Abclonal, Wuhan, China), anti-AKT (1:500, A11016, Abclonal, Wuhan, China), and anti-GAPDH (1:2000, ab181602, Abcam, Cambridge, UK). After membrane washing with TBST (ZS405-3, Zomanbio, Beijing, China), the membranes were incubated with HRP-labeled goat anti-rabbit secondary antibody (1:2000, ab205718, Abcam, Cambridge, UK) for 2 hours. Chemiluminescent signals were developed using enhanced chemiluminescence (ECL) substrate (A38554, Thermo Fisher Scientific, Massachusetts, USA), and band intensities were quantified using ImageJ (V1.8.0.112, NIH, Madison, WI, USA). Normalized to GAPDH, the relative expression levels of proteins were detected.

Cell Counting Kit-8 (CCK-8) Assay

H9c2 cells were seeded at a density of 5000 per well into 96 well plates. After processing, 10% CCK-8 reagent (HY-K0301, MCE, New Jersey, USA) was added for 3-hour incubation. The absorbance was then measured at 450 nm using a microplate reader (Thermo Fisher Scientific, Waltham, MA, USA).

Lactate Dehydrogenase (LDH) Determination

The supernatant was collected from H9c2 cell culture and cellular injury was assessed by quantifying LDH release into the supernatant. According to the manufacturer's instructions, a LDH assay kit (C0016, Beyotime, Shanghai, China) was used to measure the levels of LDH released by cells.

TdT-Mediated dUTP Nick End Labeling (TUNEL) Staining

Apoptotic cells in myocardial tissues and H9c2 cultures were identified using a TUNEL assay kit (C1086, C1089, Beyotime, Shanghai, China). Myocardial tissue sections were deparaffinized in xylene, rehydrated by gradient ethanol, and then added with proteinase K dropwise at 37°C for 20 minutes. TUNEL reaction mix (50 μL/section) was applied and incubated at 37°C in the dark for 60 minutes, followed by nuclear counterstaining with 4', 6-Diamidino-2-phenylindole (DAPI) and mounting with anti-fluorescence quenching solution. For H9c2 cells, monolayers were washed once with phosphate buffered saline (PBS) and fixed in 4% paraformaldehyde for 30 minutes. After washing again with PBS, enhanced immunostaining permeabilization buffer (P0097, Beyotime, Shanghai, China) was added and incubated at room temperature for 5 minutes. Afterwards, TUNEL reaction mix and DAPI staining solution were added. Stained samples were observed and photographed under a fluorescence microscope, and TUNEL-positive cells were quantified using ImageJ software.

Biochemical Analysis

Intracellular glutathione (GSH) and malondialdehyde (MDA) levels in H9c2 cells were quantified using the GSH assay kit (MAK364, Sigma-Aldrich, St. Louis, USA) and MDA assay kit (MAK085, Sigma-Aldrich, St. Louis, USA),

respectively, according to the manufacturer's instructions. The GSH assay is based on an enzymatic recycling method that specifically detects reduced glutathione. A chromogenic substrate is reduced by GSH to generate a colored product, which is measured at 450 nm. The assay includes 5-sulfosalicylic acid to prevent oxidation of GSH, ensuring high specificity. MDA levels were measured using the thiobarbituric acid reactive substances (TBARS) method, in which MDA reacts with thiobarbituric acid under high temperature and acidic conditions to form a red adduct, detected at 532 nm.

Intracellular Fe^{2+} Quantification

Intracellular Fe^{2+} levels were measured using an iron colorimetric assay kit (E-BC-F101, Elabscience, Wuhan, China) according to the manufacturer's instructions.

Measurement of Intracellular ROS Levels

H9c2 cells were incubated with DCFH-DA (S0033, Beyotime, China) at 37°C for 10 minutes. After washing three times with DMEM (Gibco, USA), cell images were immediately captured under a fluorescence microscope. The relative fluorescence intensity was analyzed using ImageJ.

Co-Immunoprecipitation (Co-IP)

Firstly, H9c2 cells were lysed using Pierce IP lysis buffer (87787, Thermo Fisher Scientific, Massachusetts, USA) containing a mixture of protease inhibitors (Roche, Switzerland) to extract total protein. For immunoprecipitation, lysates were incubated overnight at 4°C with anti-USP7 antibody (1:100, PA5-34911, Thermo Fisher Scientific, Massachusetts, USA), anti-PTEN antibody (1:30, ab267787, Abcam, Cambridge), or control IgG (1 μg, 30000-0-AP, Proteintech, Wuhan, China). After incubation with agarose beads, bead-antibody complexes were collected, boiled, resolved, and analyzed for protein expression in immunoprecipitated products by WB.

Deubiquitination Detection

To investigate USP7-mediated deubiquitination of PTEN, H9c2 cells were transfected or co-transfected with Myc-tagged PTEN, HA-tagged Ub, and Flag-tagged USP7 expression vectors. After 24 hours of transfection, cells were lysed using RIPA lysis buffer containing protease inhibitors, and cell debris was removed by centrifugation. The supernatant was collected for subsequent Co-IP using anti-HA magnetic beads (1:30, ab236632, Abcam, Cambridge, UK). WB sequentially probed for ubiquitinated PTEN using anti-HA (1:1000, ab236632, Abcam, Cambridge, UK), anti-Myc (1:1000, ab9106, Abcam, Cambridge, UK), and anti-Flag antibodies (1:1000, SAB4301135, Thermo Fisher Scientific, Massachusetts, USA) in the immunoprecipitated complexes. Comparative analysis of PTEN ubiquitination levels was conducted in the presence or absence of USP7.

Protein Stability Determination

To assess USP7-dependent protein stability, H9c2 cells transfected with sh-USP7 were treated with cycloheximide (CHX, 20 μg/mL, Sigma-Aldrich), a translational inhibitor, for 0, 15, 30, 60, 120, and 240 minutes. At each time point, cells were harvested and lysed for WB analysis.

Statistical Analysis

Statistical analyses were performed using GraphPad Prism 9 software. The sample size was chosen based on previous related studies.[30] Normality of data distribution was assessed using the Shapiro–Wilk test before statistical analysis. Data are presented as mean ± standard deviation (mean ± SD). Comparisons between two groups were conducted using an independent samples *t*-test; for multiple group comparisons, one-way analysis of variance (ANOVA) was applied. When overall differences were significant, Tukey's post hoc test was performed. A p-value < 0.05 was considered statistically significant. Each experiment was repeated at least three times.

Result

Sev Reduces Myocardial Cell Damage and Downregulates USP7

This study investigated the protective effects of Sev against myocardial injury in rats. A myocardial I/R injury model was established by occluding the LAD for 30 minutes, followed by 2 hours of reperfusion. First, serum cTnT levels were significantly elevated in the I/R group compared to the Sham group, but were markedly reduced after Sev treatment (Figure 1A). This indicates that Sev effectively alleviates myocardial injury, highlighting its protective role in I/R injury. Next, hemodynamic parameter analysis showed that, compared to the Sham group, the I/R group exhibited increased heart rate (HR) and shock index (SI), along with decreased left ventricular developed pressure (LVDP), maximum rates of left ventricular pressure increase (+dp/dtmax) and decrease (-dp/dtmax), and rate-pressure product (RPP), suggesting severe myocardial damage. However, Sev treatment significantly improved these parameters (Figure 1B), further confirming its cardioprotective effects. TTC staining revealed a significantly larger myocardial infarction area in the I/R group compared to the Sham group, which was markedly reduced following Sev treatment (Figure 1C). Furthermore, HE staining showed severe structural damage to cardiomyocytes in

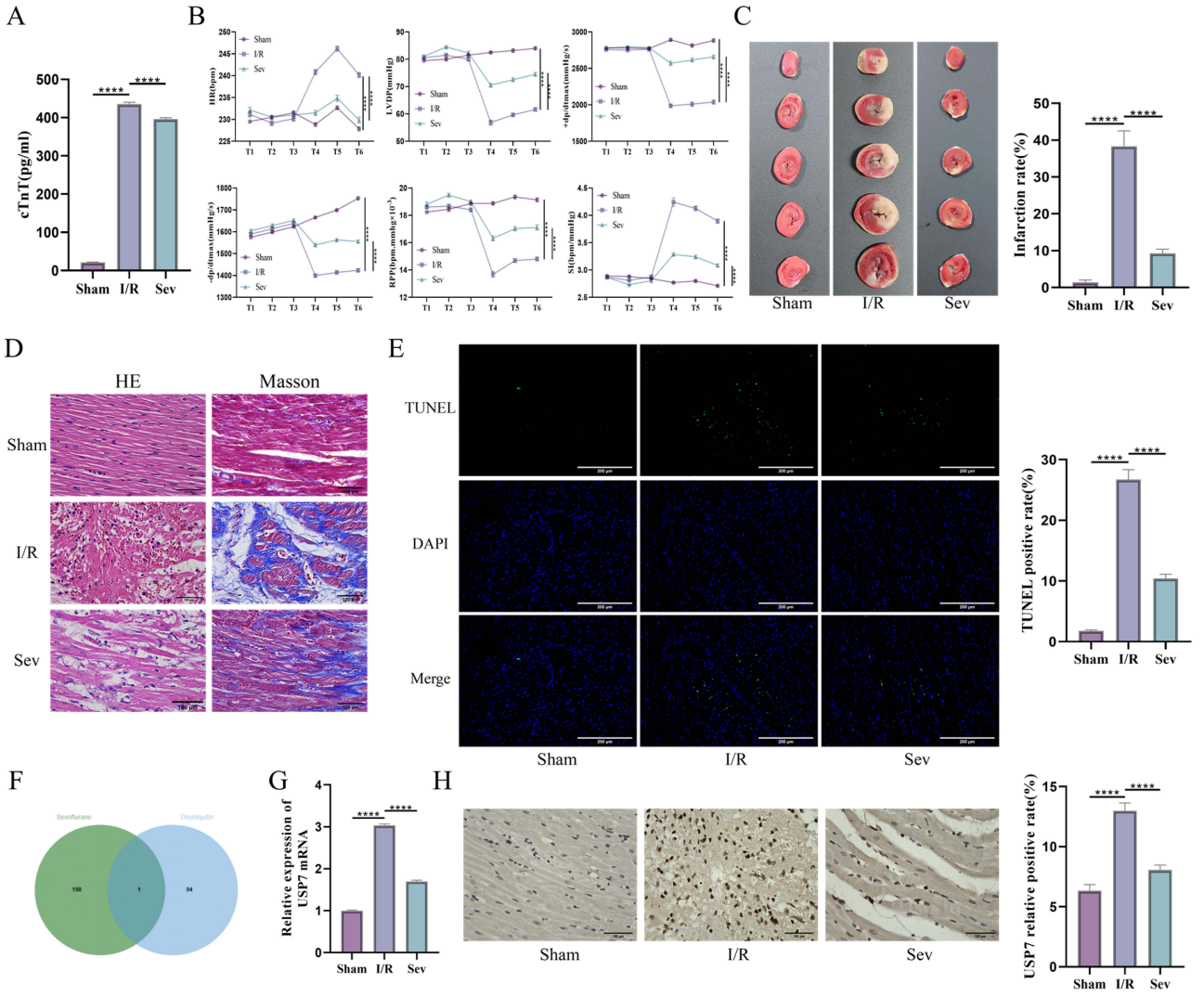

Figure 1 The protective effect of Sev on myocardial ischemia-reperfusion injury (I/R) in rats. (**A**) Serum cardiac troponin T levels; (**B**) Hemodynamic parameters, including heart rate (HR), left ventricular developed pressure (LVDP), maximal rates of left ventricular pressure increase (+dp/dtmax) and decrease (-dp/dtmax), rate-pressure product (RPP), and shock index (SI); (**C**) Myocardial infarct size measured by TTC staining; (**D**) Histological evaluation of myocardial tissue damage and fibrosis using HE and Masson staining. The scale bar is 100 μm; (**E**) TUNEL assay to determine the rate of myocardial cell apoptosis. The scale bar is 200 μm; (**F**) Prediction of the potential target USP7 of Sev using the SuperPred and Ubibrowser 2.0 databases; (**G**) RT-qPCR analysis of USP7 mRNA expression; (**H**) IHC detection of USP7 protein-positive expression changes. The scale bar is 100 μm. Data were analyzed using one-way ANOVA (**A**, **C**, **E**, **G** and **H**) or two-way ANOVA (**B**), followed by Tukey's post-hoc test. N=10 (**A** and **B**), N=5 (**C**–**E** and **G**–**H**), ****p < 0.0001.

https://doi.org/10.2147/DDDT.S524019

the I/R group, which was significantly alleviated by Sev (Figure 1D). Masson staining results demonstrated a substantial increase in myocardial fibrosis in the I/R group compared to the Sham group, which was significantly reduced after Sev treatment (Figure 1D). TUNEL staining revealed elevated apoptosis rates in myocardial tissue in the I/R group compared to the Sham group, which were reversed by Sev treatment (Figure 1E). These findings indicate that Sev mitigates I/R-induced injury by inhibiting cardiomyocyte apoptosis. To further explore the protective mechanism of Sev, we predicted its potential downstream targets using chemoinformatics methods. The structure of Sev was input into the SuperPred database (https://prediction.charite.de/index.php) to obtain candidate proteins potentially binding to Sev based on molecular structural similarity. Considering the critical role of deubiquitination in myocardial injury, we focused on targets related to deubiquitinases. A list of known deubiquitinases was extracted from the Ubibrowser 2.0 database (http://ubibrowser.bio-it.cn/ubibrowser_v3/home/index). Subsequently, the online tool jvenn (https://jvenn.toulouse.inrae.fr/app/example.html) was used to generate a Venn diagram for intersection analysis. USP7 was identified as a potential target of Sev (Figure 1F), providing a basis for subsequent mechanistic studies. RT-qPCR and IHC analyses revealed significantly elevated USP7 expression in the I/R group compared to the Sham group, which was markedly downregulated following Sev treatment (Figure 1G and H). These results suggest that Sev effectively alleviates myocardial injury in rats, potentially by downregulating USP7 expression.

Overexpression of USP7 Inhibits the Protective Effect of Sev on Cardiomyocytes

To further explore the protective effects of Sev against myocardial injury and its molecular mechanisms, we constructed a USP7 overexpression cell model. The overexpression of USP7 was validated through RT-qPCR and WB analysis (Figure 2A and B). Subsequently, we induced hypoxia/reoxygenation (H/R) in H9c2 cells to establish a myocardial injury cell model. The results showed that cell viability in the H/R group was significantly lower than in the Control group, whereas Sev treatment markedly improved cell viability, demonstrating its protective effects on cardiomyocytes. However, the increase in cell viability induced by Sev was inhibited by USP7 overexpression (Figure 2C). Furthermore, the lactate dehydrogenase (LDH) release assay revealed that LDH levels were significantly elevated in the H/R group compared to the Control group. Sev treatment reversed this

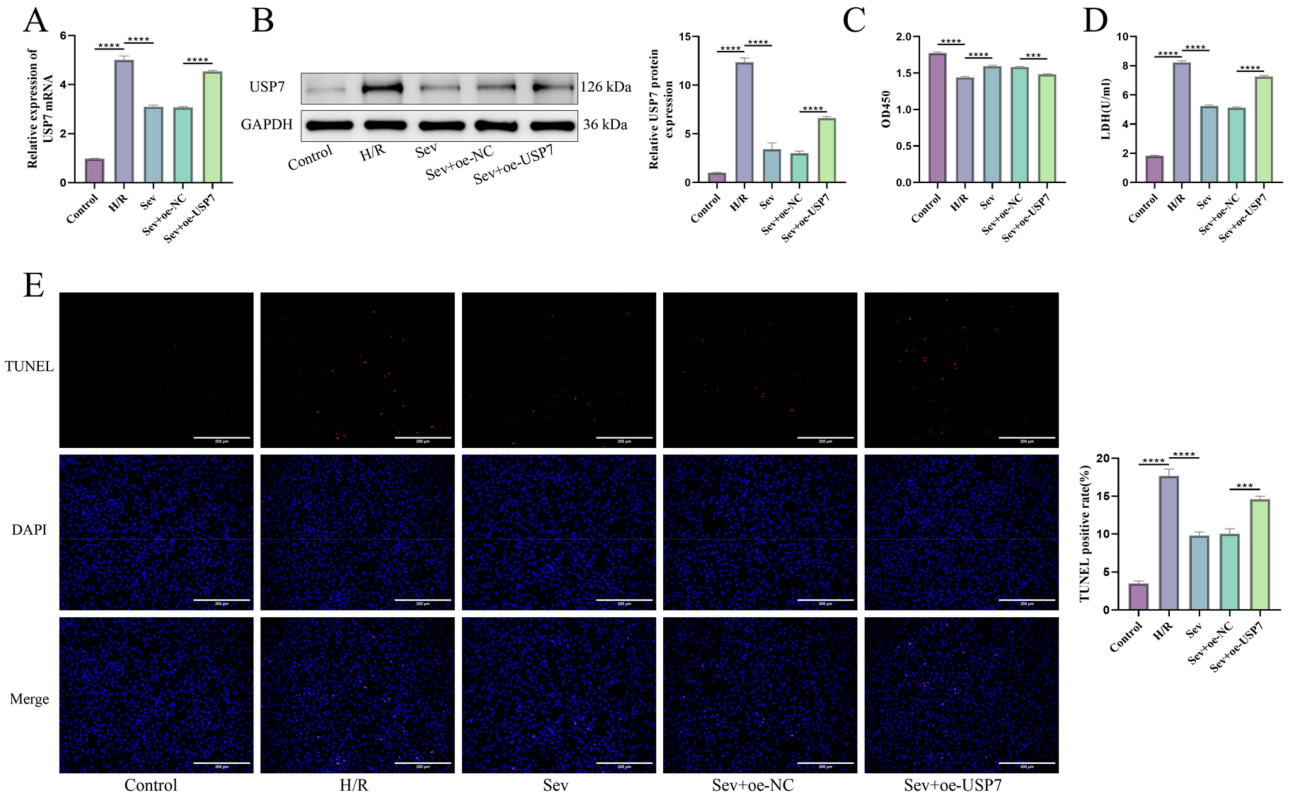

Figure 2 Overexpression of USP7 inhibits the protective effect of Sev on H9c2 cells under hypoxia/reoxygenation (H/R) injury. (**A**) RT-qPCR analysis of USP7 mRNA levels; (**B**) WB analysis of USP7 protein expression levels; (**C**) CCK-8 assay to evaluate cell viability; (**D**) LDH release assay to assess cell damage; (**E**) TUNEL assay to determine the proportion of apoptotic cells. The scale bar is 200 μm. Data were analyzed using one-way ANOVA followed by Tukey's post-hoc test. N=5, ***p < 0.001, ****p < 0.0001.

increase, but USP7 overexpression led to a resurgence of LDH levels (Figure 2D). TUNEL staining further indicated that the proportion of apoptotic cells was significantly higher in the H/R group compared to the Control group. Sev treatment reduced cell apoptosis, but USP7 overexpression again enhanced apoptosis induced by H/R (Figure 2E). These findings suggest that Sev exerts its protective effects by inhibiting USP7, thereby reducing apoptosis in cardiomyocytes.

Overexpression of USP7 Weakens the Reversal Effect of Sev on Iron Death in Cardiomyocytes

USP7 is a deubiquitinating enzyme, and growing evidence suggests that USP7 is closely associated with ferroptosis by regulating the stability of antioxidant enzymes.[15] Therefore, we hypothesized that Sev might protect against myocardial injury by inhibiting USP7-mediated ferroptosis. Compared to the Control group, the H/R group exhibited significantly reduced GSH levels, along with elevated MDA content and ROS levels, indicating oxidative stress in the cells. Sev treatment significantly increased GSH levels, decreased MDA content, and reduced ROS levels, suggesting that Sev alleviates oxidative stress in cardiomyocytes. However, in the Sev + oe-USP7 group, GSH levels decreased again, while MDA and ROS levels increased compared to the Sev + oe-NC group (Figure 3A and B), indicating that USP7 overexpression reinstated oxidative stress in cardiomyocytes. Additionally, intracellular Fe^{2+} levels were significantly increased in the H/R group compared to the Control group. Sev treatment reduced Fe^{2+} levels, but USP7 overexpression in the Sev + oe-USP7 group led to a subsequent increase in Fe^{2+} levels (Figure 3C). RT-qPCR and Western blot analyses further revealed that ferroptosis inhibitors GPX4 and FTH1 were significantly downregulated in the H/R group compared to the Sham group. Sev treatment upregulated the expression of GPX4 and FTH1, but their levels decreased again upon USP7 overexpression (Figure 3D and E). These findings collectively demonstrate that Sev inhibits H/R-induced ferroptosis in cardiomyocytes, and this effect is closely related to the downregulation of USP7.

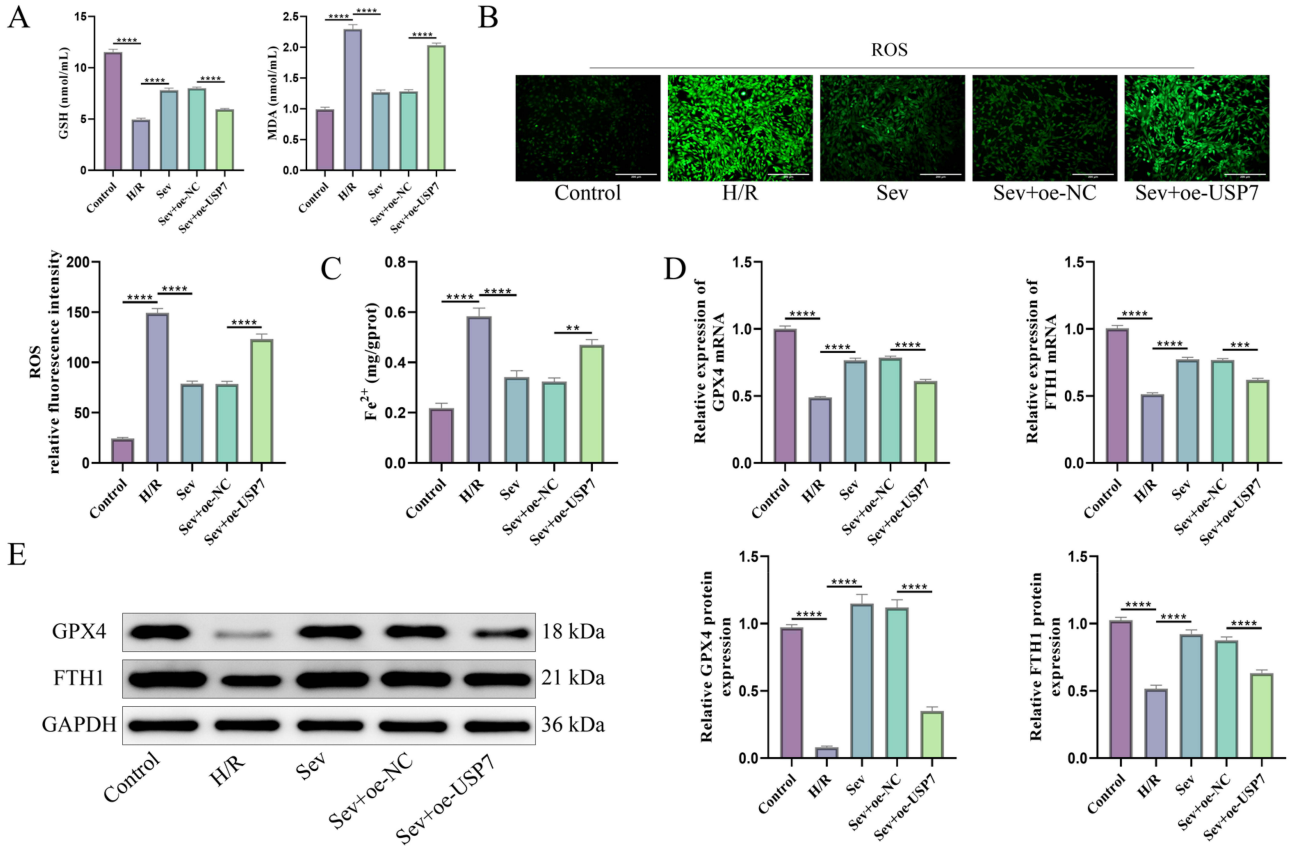

Figure 3 Sev reduces oxidative stress and inhibits ferroptosis in H9c2 cells by suppressing USP7. (**A**) Levels of GSH and MDA to assess oxidative stress; (**B**) ROS levels to evaluate intracellular reactive oxygen species. The scale bar is 200 μm; (**C**) Fe^{2+} levels to measure intracellular iron content; (**D**) RT-qPCR analysis of mRNA expression of ferroptosis inhibitors GPX4 and FTH1; (**E**) WB analysis of GPX4 and FTH1 protein expression. Data are analyzed using one-way ANOVA followed by Tukey's post hoc test. N=5, **p < 0.01, ***p < 0.001, ****p < 0.0001.

https://doi.org/10.2147/DDDT.S524019

USP7 Mediates PTEN Deubiquitination Pathway

To further explore the mechanism of Sev, we predicted the downstream targets of USP7 using the Ubibrowser database and intersected these with ferroptosis-promoting targets obtained from the FerrDb database (http://www.zhounan.org/ferrdb/current/#), identifying 11 overlapping targets, including CCDC6, FOXO4, HIF1A, MDM2, MDM4, MYCN, PPARG, PTEN, SOCS1, TP53, and YAP1 (Figure 4A). Literature suggests that PTEN regulates ferroptosis through the PI3K/AKT pathway. Western blot analysis showed a significant upregulation of PTEN protein and downregulation of PI3K and AKT proteins in the I/R group compared to the Sham group. Sev treatment reduced PTEN protein expression while increasing PI3K and AKT levels (Figure 4B). Similarly, in cellular experiments, the H/R group displayed elevated PTEN expression and decreased PI3K and AKT levels compared to the Control group. These changes were reversed by Sev treatment, but PTEN levels were again upregulated, and PI3K and AKT levels reduced upon USP7 overexpression (Figure 4C). These results suggest that Sev might exert its protective effect on the myocardium by regulating PTEN expression via USP7. Next, we validated the interaction between USP7 and PTEN using a Co-IP assay (Figure 4D). Additionally, H9c2 cells were transfected with plasmids encoding HA-Ub, Myc-PTEN, and Flag-USP7. The analysis confirmed an interaction between PTEN and Ub, and USP7 significantly reduced the binding of PTEN to Ub (Figure 4E), indicating that USP7 mediates the deubiquitination of PTEN. Furthermore, CHX treatment revealed that knockdown of USP7 shortened the half-life of the PTEN protein (Figure 4F), highlighting that USP7 mediates PTEN deubiquitination and promotes its protein stability.

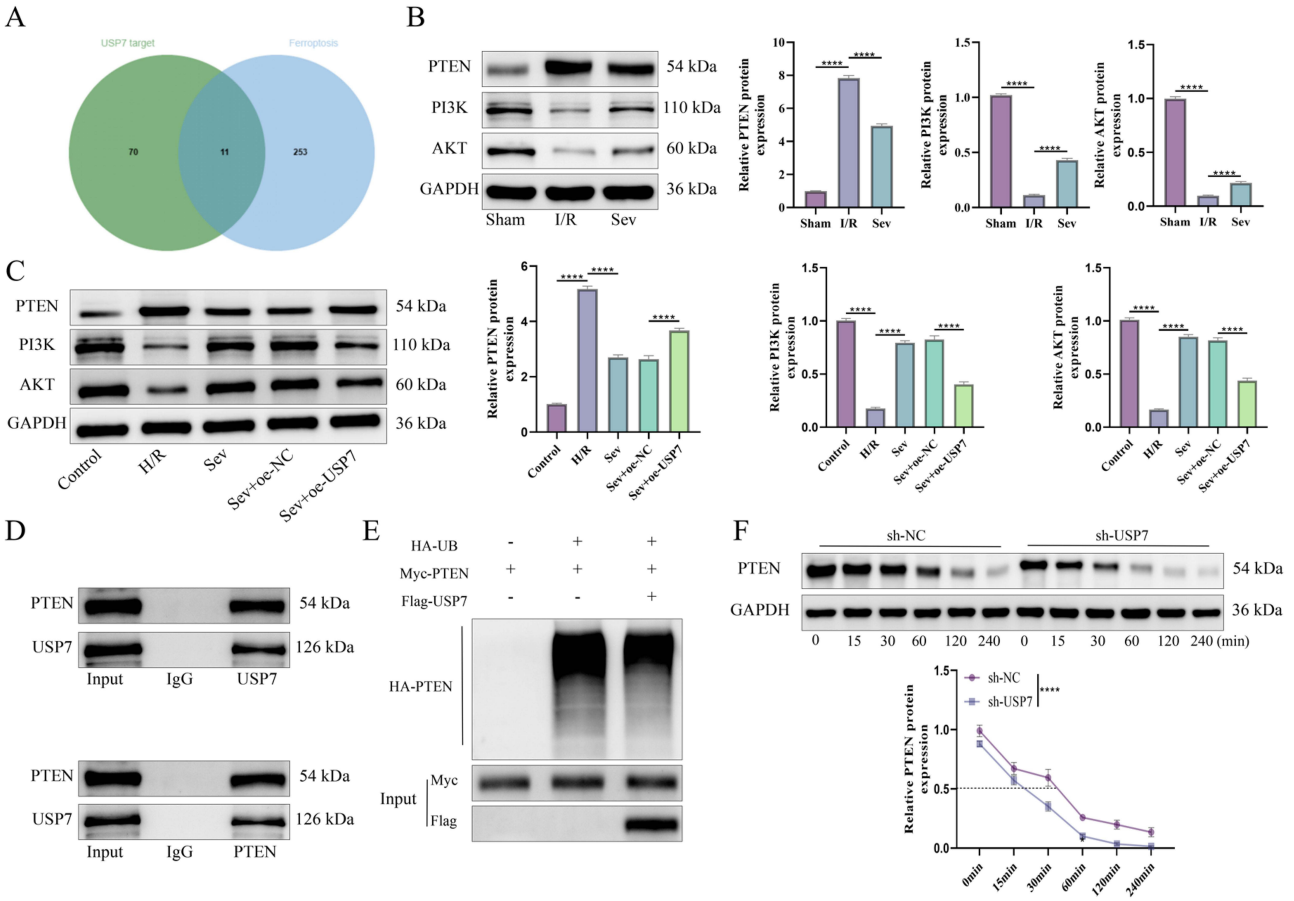

Figure 4 USP7 regulates PTEN stability through deubiquitination, contributing to the protective effects of Sev against ferroptosis. (**A**) Intersection of USP7 downstream targets predicted by the Ubibrowser database and ferroptosis-related targets identified from the Ferrdb database. (**B**) WB analysis of PTEN, PI3K, and AKT protein levels in myocardial tissues of I/R rats. (**C**) WB analysis of PTEN, PI3K, and AKT protein expression in H9c2 cells. (**D**) Co-IP assay confirming the interaction between USP7 and PTEN. (**E**) Analysis of PTEN ubiquitination levels following co-transfection with HA-Ub, Myc-PTEN, and Flag-USP7 plasmids. (**F**) Effect of USP7 knockdown on PTEN protein half-life after CHX treatment. Data were analyzed using one-way ANOVA (**B** and **C**) and two-way ANOVA (**F**), followed by Tukey's post hoc test. N=5, ****p < 0.0001.

 https://doi.org/10.2147/DDDT.S524019

Sev Alleviates Myocardial Cell Iron Death Mechanism by Inhibiting USP7 Mediated PTEN/PI3K/AKT

PTEN's primary function is to inhibit the PI3K/Akt signaling pathway, thereby regulating cell growth, proliferation, and survival. This study aims to further confirm that Sev alleviates ferroptosis in H9c2 cells by suppressing USP7-mediated PTEN deubiquitination and subsequently activating the PI3K/Akt pathway. First, cells were treated with USP7 overexpression and PTEN knockdown. RT-qPCR and WB results showed that sh-PTEN 1 achieved the best knockdown efficiency (Figure 5A and B), and subsequent experiments were conducted using sh-PTEN 1. Following H/R treatment, cell viability was significantly increased in the Sev + oe-USP7 + sh-PTEN group compared to the Sev + oe-USP7 + sh-NC group (Figure 5C). Additionally, LDH release and TUNEL assays demonstrated that PTEN knockdown alleviated cellular damage (Figure 5D and E). Ferroptosis-related indicators showed that GSH levels were significantly elevated, while MDA and ROS levels were reduced after PTEN knockdown (Figure 5F and G), indicating an amelioration of oxidative stress. Furthermore, intracellular Fe^{2+} levels were markedly decreased (Figure 5H), providing additional evidence of reduced ferroptosis. Further analysis revealed that PTEN knockdown enhanced the activity of PI3K and AKT proteins, while increasing the expression levels of GPX4 and FTH1 proteins (Figure 5I). These findings suggest that USP7-mediated PTEN deubiquitination inhibits PI3K/Akt pathway activation, whereas PTEN knockdown restores the pathway's activity, thereby mitigating ferroptosis in cardiomyocytes.

Sev Inhibits Myocardial Injury in I/R Rats by Suppressing USP7/PTEN

In vivo experiments further confirmed that Sev alleviates ferroptosis in cardiomyocytes by inhibiting USP7-mediated PTEN deubiquitination and activating the PI3K/AKT signaling pathway, consistent with the in vitro findings. WB

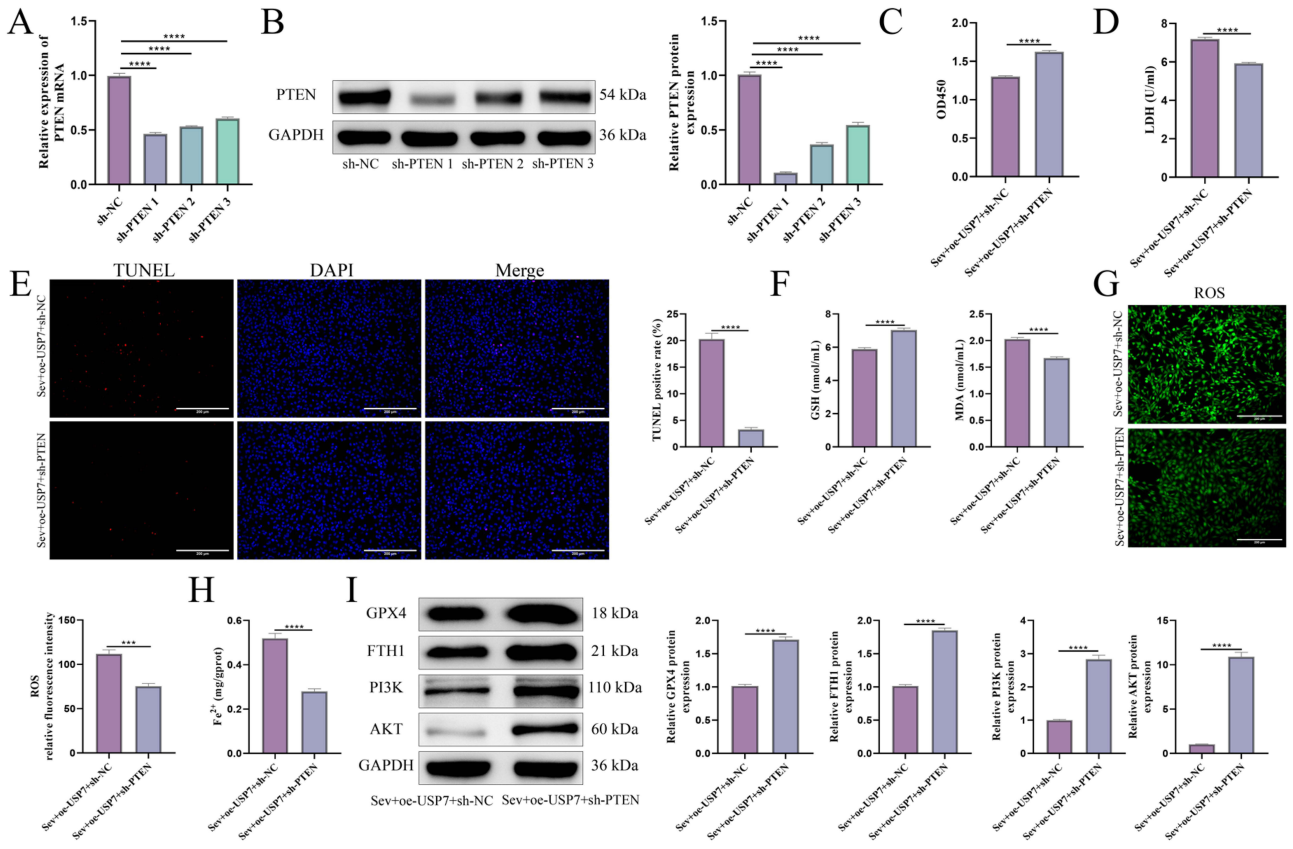

Figure 5 Knockdown of PTEN alleviates ferroptosis in H9c2 cells induced by USP7 overexpression through activation of the PI3K/Akt pathway. (**A**) RT-qPCR analysis of PTEN knockdown efficiency; (**B**) Western blot analysis of PTEN knockdown levels; (**C**) CCK-8 assay to assess cell viability; (**D**) LDH release assay to evaluate cellular damage; (**E**) TUNEL assay to measure apoptosis rates. The scale bar is 200 μm; (**F**) GSH and MDA assays to evaluate oxidative stress levels; (**G**) ROS detection assay. The scale bar is 200 μm; (**H**) Measurement of Fe^{2+} levels to assess intracellular iron content; (**I**) Western blot analysis of PI3K, AKT, GPX4, and FTH1 protein expression. Data were analyzed using one-way ANOVA followed by Tukey's post hoc test. N=5, ***p < 0.001, ****p < 0.0001.

https://doi.org/10.2147/DDDT.S524019

analysis revealed that overexpression of USP7 significantly increased USP7 and PTEN protein levels while decreasing PI3K and AKT protein expression. Conversely, PTEN knockdown significantly reduced PTEN protein levels, restored PI3K and AKT protein expression, and showed no significant effect on USP7 protein levels (Figure 6A). These results suggest that USP7 overexpression promotes PTEN protein expression, but changes in PTEN protein levels do not affect USP7 protein levels. Further findings showed that serum cTnT levels were elevated in the Sev + oe-USP7 group compared to the Sev + oe-NC group, while PTEN knockdown reversed this increase (Figure 6B). Hemodynamic parameters demonstrated that, compared to the Sev + oe-NC group, heart rate (HR) and stroke index (SI) increased in the Sev + oe-USP7 group, whereas left ventricular developed pressure (LVDP), +dp/dtmax, -dp/dtmax, and rate-pressure product (RPP) decreased, indicating aggravated myocardial injury. However, PTEN knockdown reversed these changes (Figure 6C). TTC staining revealed a larger myocardial infarct size in the Sev + oe-USP7 group compared to the Sev + oe-NC group, which was reduced after PTEN knockdown (Figure 6D). HE staining showed that the myocardial structure in the Sev + oe-USP7 group was severely damaged compared to the Sev + oe-NC group, whereas PTEN knockdown mitigated this damage (Figure 6E). Masson staining indicated increased myocardial fibrosis in the Sev + oe-USP7 group compared to the Sev + oe-NC group, while PTEN knockdown improved fibrosis (Figure 6E). TUNEL staining demonstrated increased apoptosis in the Sev + oe-USP7 group compared to the Sev + oe-NC group, which decreased upon PTEN knockdown (Figure 6F). These results indicate the critical role of USP7-mediated PTEN regulation in Sev's therapeutic effect on myocardial I/R injury. To further validate the involvement of this molecular mechanism in ferroptosis, we conducted additional in vivo experiments. WB analysis of various groups revealed that GPX4 and FTH1 protein levels were significantly downregulated in the Sev + oe-USP7 group compared to the Sev + oe-NC group, while PTEN knockdown reversed these changes (Figure 6G). These findings suggest that PTEN knockdown can partially reverse the cell damage caused by USP7 overexpression. In conclusion, Sev alleviates cardiomyocyte damage by enhancing antioxidant enzyme expression and activating the PI3K/AKT signaling pathway.

Discussion

Acute myocardial infarction (MI) is the leading cause of death and disability worldwide, and the preferred treatment is to salvage myocardial injury through reperfusion.[31] However, myocardial I/R injury may lead to serious cardiovascular complications and adverse clinical outcomes.[32] Nowadays, increasing evidence suggests that Sev has vasodilatory effects,[33] which can improve myocardial blood flow, enhance myocardial oxygen supply, and help alleviate myocardial ischemia.[34] There are also literature reports that Sev affects the cardioprotective mechanism by regulating the activity of deubiquitinase.[29] At the same time, we found the direct downstream target USP7 of Sev in the SuperPred database, which is considered a negative regulatory factor in myocardial I/R injury. It increases myocardial I/R injury by promoting cardiomyocyte apoptosis and exacerbating oxidative stress.[35] Based on this, we reasonably assume that Sev has a protective effect on myocardial I/R injury by targeting USP7. Therefore, we aim to elucidate the possible mechanism of Sev in protecting against myocardial I/R injury and explore in depth the correlation between USP7 and its downstream genes.

Sev has multiple pharmacological properties, including volatility, safety, and non flammability,[36] which highlight its potential clinical application value in the treatment of coronary artery disease. Previous studies have shown that Sev can alleviate myocardial injury and repair cardiac function, thereby alleviating myocardial I/R injury.[37] However, its specific function in myocardial I/R injury and myocardial cells is still unclear. To investigate the effect of Sev on myocardial I/R injury, we constructed an in vivo rat model of myocardial I/R injury and an in vitro H9c2 cell model of H/R, both of which were treated with Sev. It was found that Sev has a relieving effect on the deterioration of hemodynamic indicators, myocardial injury, fibrosis, and cell apoptosis caused by myocardial I/R injury. At the same time, Sev has a blocking effect on the decrease in cell viability, apoptosis, and necrosis caused by H/R treatment of H9c2 cells. Similarly, previous studies have shown that Sev can reduce the size of myocardial infarction and rescue myocardial cell damage.[38] Li et al confirmed that Sev treatment improved cardiac dysfunction, pathological damage to myocardial tissue, and reduced myocardial apoptotic cells after myocardial I/R injury.[39] Based on all the findings and evidence mentioned above, Sev does indeed have potential therapeutic effects in treating myocardial I/R injury.

Another finding in our study is that the expression of USP7 mRNA and protein is significantly increased in myocardial I/R injury. Overexpression of USP7 promotes ferroptosis, while after Sev treatment, USP7 expression is

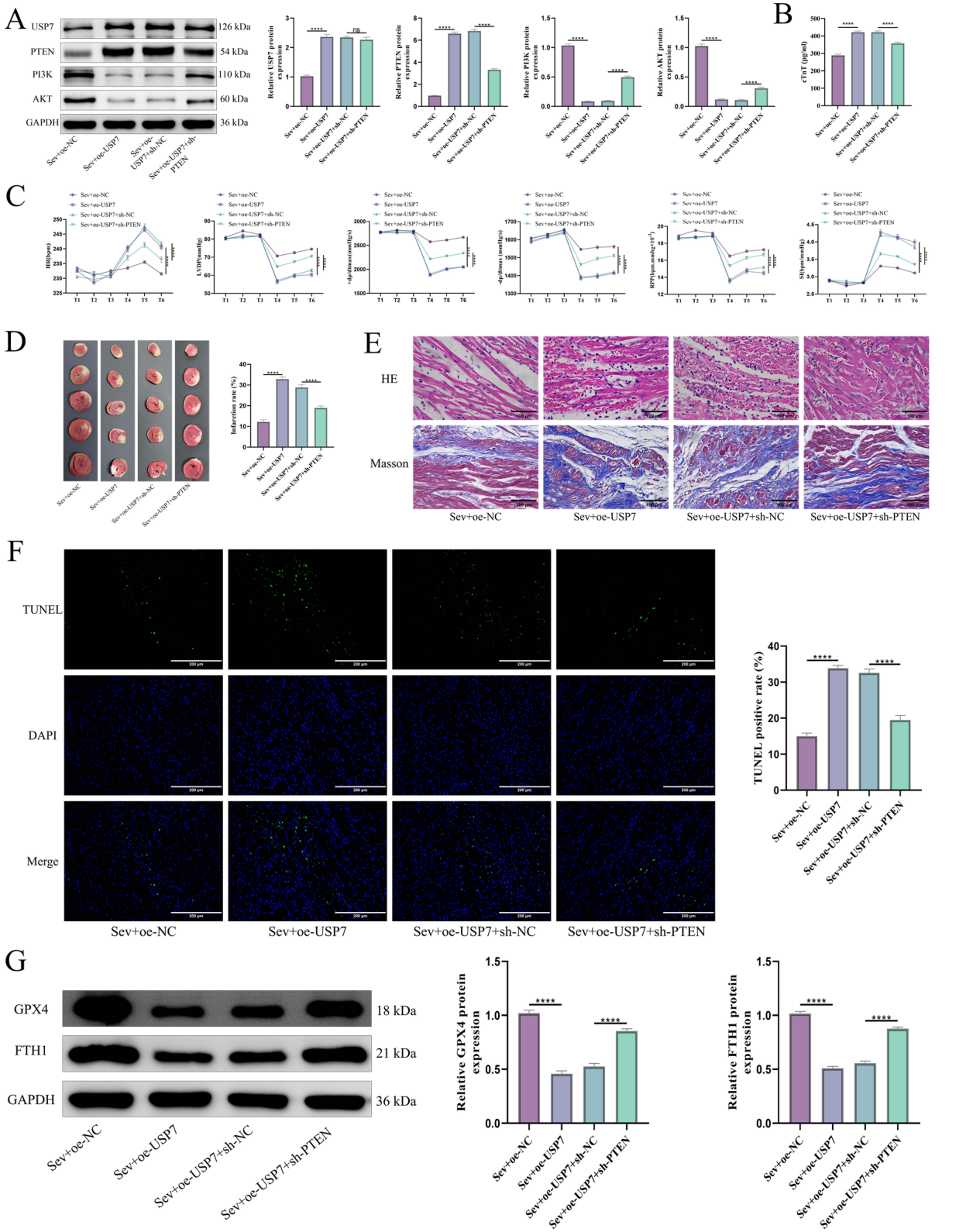

Figure 6 Validation of Sev's protective effect against ferroptosis in cardiomyocytes through inhibition of USP7-mediated PTEN deubiquitination and activation of the PI3K/AKT signaling pathway in vivo. (**A**) Western blot analysis of USP7, PTEN, PI3K, and AKT protein expression in myocardial tissues from different treatment groups; (**B**) Serum cTnT levels; (**C**) Hemodynamic parameters, including heart rate (HR), stroke index (SI), left ventricular diastolic pressure (LVDP), +dp/dtmax, -dp/dtmax, and rate-pressure product (RPP); (**D**) Myocardial infarct size assessed by TTC staining; (**E**) Structural damage to cardiomyocytes observed by HE staining and. Myocardial fibrosis evaluated by Masson staining. The scale bar is 100 μm; (**F**) Cardiomyocyte apoptosis detected by TUNEL staining. The scale bar is 200 μm; (**G**) Expression levels of ferroptosis-related proteins GPX4 and FTH1 in myocardial tissue determined by Western blot analysis. Data were analyzed using one-way ANOVA (**A**, **B**, **D**, **F** and **G**) and two-way ANOVA (**C**), followed by Tukey's post hoc test. N=10 (**B** and **C**), N=5 (**A** and **D**–**G**), ns $p > 0.05$, ****$p < 0.0001$.

https://doi.org/10.2147/DDDT.S524019

downregulated and ferroptosis is inhibited. Previous evidence suggests a close association between USP7 and ferroptosis.[40] Inhibition of USP7 can reduce iron deposition and suppress oxidative stress, thereby inhibiting iron death in myocardial ischemia.[19] In addition, literature reports that Sev alleviates myocardial I/R injury in rats by regulating the expression of deubiquitinase.[29] However, it has not been reported whether Sev alleviates iron death and myocardial dysfunction caused by myocardial I/R injury by downregulating the expression of USP7. Therefore, in this study, we continued to overexpress USP7 in myocardial I/R injury rats treated with Sev, and used Sev treatment and transfection of oe-USP7 in H/R-induced H9c2 cells. The results showed that the hemodynamic indicators of rats deteriorated, myocardial infarction area expanded, myocardial re injury occurred, fibrosis worsened, and accompanied by a large number of cell apoptosis. In addition, the expression of iron death inhibitory proteins GPX4 and FTH1 also decreased. At the same time, H9c2 cell activity was inhibited, apoptosis rate increased, oxidative stress and iron death were abnormally activated, and ROS accumulation worsened. It is known that ubiquitin proteasome is an important participant in myocardial I/R injury,[18] and our findings suggest that Sev can downregulate USP7 to alleviate myocardial I/R injury. In summary, these findings and data suggest that overexpression of USP7 weakens the protective effect of Sev in iron death mediated myocardial I/R injury. Although the precise mechanism by which Sev downregulates USP7 expression has not been fully elucidated, accumulating evidence suggests that inhalational anesthetics can regulate gene expression through transcriptional and post-transcriptional mechanisms, including epigenetic modifications and the involvement of non-coding RNAs.[41,42] We plan to conduct further experiments to explore the molecular mechanisms by which Sev regulates USP7. PTEN protein plays an important regulatory role in myocardial I/R injury,[43] but its stability and function are regulated by deubiquitinase.[44] The deubiquitinase increases the stability of PTEN by removing its ubiquitin chain and inhibiting its degradation,[45] thereby affecting the activity of the PI3K/AKT signaling pathway.[44] As a negative regulator of the PI3K/AKT signaling pathway, PTEN plays a positive role in the apoptosis, cell survival, and repair functions of cardiomyocytes.[46] The PI3K/AKT pathway also participates in regulating iron absorption and storage, affecting intracellular iron levels.[2] However, it is still unknown whether USP7 regulates myocardial cell apoptosis and ferroptosis by stabilizing PTEN in myocardial I/R injury. Therefore, we speculated and validated the interaction between USP7 and PTEN in subsequent experiments, confirming that USP7 mediates PTEN ubiquitination. To investigate whether PTEN is involved in the protective mechanism of Sev against myocardial I/R injury, we added Sev to H9c2 cells treated with H/R and co transfected them with oe USP7 and sh PTEN. The results showed that H9c2 cell activity was enhanced, apoptosis rate was decreased, oxidative stress and ferroptosis were inhibited, and ROS was downregulated. In addition, the PI3K/AKT signaling pathway was also activated. Based on this, we also conducted in vivo validation, and the results were consistent with those in vitro. In addition, Xiong et al also confirmed that overexpression of PTEN further affects the apoptosis and injury process of cardiomyocytes.[47] In summary, these pieces of evidence suggest that PTEN is involved in the protective mechanism of Sev against myocardial I/R injury, and targeted regulation of PTEN may provide new strategies for further enhancing Sev's cardioprotective effects. However, increasing evidence indicates that Nrf2 and p53 play important roles in regulating oxidative stress and ferroptosis.[48] Comparing and integrating these alternative pathways can help provide a more comprehensive understanding of the complex regulatory mechanisms involved in myocardial I/R injury and ferroptosis, and may reveal additional potential therapeutic targets. Future studies should focus on the interactions and regulatory relationships between these signaling pathways and the USP7/PTEN/PI3K/AKT axis in the cardioprotective effects of Sev. Furthermore, the feasibility of targeting the USP7/PTEN axis as a therapeutic strategy in clinical settings remains insufficiently explored. The potential applications of Sev beyond anesthesia, particularly in perioperative myocardial protection, also require further evaluation. Future studies should focus on these aspects to facilitate the clinical translation of Sev and expand its use in cardiovascular protection.

However, this study is mainly based on in vitro cell and healthy animal models, and the specific regulatory role of the USP7-mediated PTEN/PI3K/AKT pathway in the cardioprotective effect of Sev has not been validated in humans or in animals with pre-existing comorbidities such as diabetes and dyslipidemia. Additionally, gene knockdown was achieved by systemic delivery via tail vein injection of AAV, which may lead to gene modulation in multiple tissues beyond the heart. This systemic approach could introduce extracardiac effects that potentially contribute to the observed cardioprotective outcomes. These factors represent limitations of the current study. Therefore, future research should include disease models

with relevant risk factors and focus on further validation through tissue-specific approaches, clinical trials, and large-scale patient data to clarify the optimal application of Sev in cardiac protection and to evaluate its safety and efficacy.

Conclusion

In summary, our research results indicate that Sev inhibits USP7 mRNA and protein expression, regulates PTEN deubiquitination modification, and activates the PI3K/AKT pathway, thereby reducing iron death in cardiomyocytes and alleviating I/R-induced cardiomyocyte injury and apoptosis. This study may provide new insights into the potential therapeutic significance of Sev in myocardial protection.

Data Sharing Statement

The data that support the findings of this study are available from the corresponding author upon reasonable request.

Ethics Statement

This study was approved by the Animal Committee of Hunan Evidence-based Biotechnology Co., Ltd (Ethics Number: XZ2024013).

Funding

No funding was received.

Disclosure

The authors report no conflicts of interest in this work.

References

1. Tian H, Zhao X, Zhang Y, Xia Z. Abnormalities of glucose and lipid metabolism in myocardial ischemia-reperfusion injury. *Biomed Pharmacother*. 2023;163:114827. doi:10.1016/j.biopha.2023.114827
2. Yi J, Zhu J, Wu J, Thompson CB, Jiang X. Oncogenic activation of PI3K-AKT-mTOR signaling suppresses ferroptosis via SREBP-mediated lipogenesis. *Proc Natl Acad Sci U S A*. 2020;117(49):31189–31197. doi:10.1073/pnas.2017152117
3. Zou R, Shi W, Qiu J, et al. Empagliflozin attenuates cardiac microvascular ischemia/reperfusion injury through improving mitochondrial homeostasis. *Cardiovasc Diabetol*. 2022;21(1):106. doi:10.1186/s12933-022-01532-6
4. Liu Y, Li X, Sun T, Li T, Li Q. Pyroptosis in myocardial ischemia/reperfusion and its therapeutic implications. *Eur J Pharmacol*. 2024;971:176464. doi:10.1016/j.ejphar.2024.176464
5. Qu Z, Pang X, Mei Z, et al. The positive feedback loop of the NAT10/Mybbp1a/p53 axis promotes cardiomyocyte ferroptosis to exacerbate cardiac I/R injury. *Redox Biol*. 2024;72:103145. doi:10.1016/j.redox.2024.103145
6. Cai W, Liu L, Shi X, et al. Alox15/15-HpETE aggravates myocardial ischemia-reperfusion injury by promoting cardiomyocyte ferroptosis. *Circulation*. 2023;147(19):1444–1460. doi:10.1161/CIRCULATIONAHA.122.060257
7. Xiang Q, Yi X, Zhu XH, Wei X, Jiang DS. Regulated cell death in myocardial ischemia-reperfusion injury. *Trends Endocrinol Metab*. 2024;35(3):219–234. doi:10.1016/j.tem.2023.10.010
8. Yi T, Wang N, Huang J, et al. A sleep-specific midbrain target for sevoflurane anesthesia. *Adv Sci*. 2023;10(15):e2300189. doi:10.1002/advs.202300189
9. An L, Zhong Y, Tan J, et al. Sevoflurane exerts protection against myocardial ischemia-reperfusion injury and pyroptosis through the circular RNA PAN3/microRNA-29b-3p/stromal cell-derived factor 4 axis. *Int Immunopharmacol*. 2023;120:110219. doi:10.1016/j.intimp.2023.110219
10. Fang FQ, Sun JH, Wu QL, et al. Protective effect of sevoflurane on vascular endothelial glycocalyx in patients undergoing heart valve surgery: a randomised controlled trial. *Eur J Anaesthesiol*. 2021;38(5):477–486. doi:10.1097/EJA.0000000000001429
11. Bie X, Ao J, Zhu D. Sevoflurane attenuates myocardial ischemia/reperfusion injury by up-regulating microRNA-99a and down-regulating BRD4. *Acta Cir Bras*. 2023;38:e383123. doi:10.1590/acb383123
12. Wu Q, Wang H, He F, et al. Depletion of microRNA-92a enhances the role of sevoflurane treatment in reducing myocardial ischemia-reperfusion injury by upregulating KLF4. *Cardiovasc Drugs Ther*. 2023;37(6):1053–1064. doi:10.1007/s10557-021-07303-x
13. Ali A, Raja R, Farooqui SR, Ahmad S, Banerjea AC. USP7 deubiquitinase controls HIV-1 production by stabilizing Tat protein. *Biochem J*. 2017;474(10):1653–1668. doi:10.1042/BCJ20160304
14. Xiang M, Liang L, Kuang X, et al. Pharmacological inhibition of USP7 suppresses growth and metastasis of melanoma cells in vitro and in vivo. *J Cell Mol Med*. 2021;25(19):9228–9240. doi:10.1111/jcmm.16834
15. Wang C, Zhu Y, Zhu X, Chen R, Zhang X, Lian N. USP7 regulates HMOX-1 via deubiquitination to suppress ferroptosis and ameliorate spinal cord injury in rats. *Neurochem Int*. 2023;168:105554. doi:10.1016/j.neuint.2023.105554
16. Dong B, Ding C, Xiang H, et al. USP7 accelerates FMR1-mediated ferroptosis by facilitating TBK1 ubiquitination and DNMT1 deubiquitination after renal ischemia-reperfusion injury. *Inflamm Res*. 2022;71(12):1519–1533. doi:10.1007/s00011-022-01648-1
17. Li J, Cao F, Yin HL, et al. Ferroptosis: past, present and future. *Cell Death Dis*. 2020;11(2):88. doi:10.1038/s41419-020-2298-2

18. Tang LJ, Zhou YJ, Xiong XM, et al. Ubiquitin-specific protease 7 promotes ferroptosis via activation of the p53/TfR1 pathway in the rat hearts after ischemia/reperfusion. *Free Radic Biol Med*. 2021;162:339–352. doi:10.1016/j.freeradbiomed.2020.10.307
19. Yang D, Zhang T, Qu H, et al. Inhibition of ubiquitin-specific protease 7 ameliorates ferroptosis-mediated myocardial infarction by contrasting oxidative stress: an in vitro and in vivo analysis. *Cell Signal*. 2024;124:111423. doi:10.1016/j.cellsig.2024.111423
20. Xu Q, Liu M, Gu J, et al. Ubiquitin-specific protease 7 regulates myocardial ischemia/reperfusion injury by stabilizing Keap1. *Cell Death Discov*. 2022;8(1):291. doi:10.1038/s41420-022-01086-2
21. Mao X, Xu J, Xiao M, et al. ARID3A enhances chemoresistance of pancreatic cancer via inhibiting PTEN-induced ferroptosis. *Redox Biol*. 2024;73:103200. doi:10.1016/j.redox.2024.103200
22. Li X, Yang P, Hou X, Ji S. Post-translational modification of PTEN protein: quantity and activity. *Oncol Rev*. 2024;18:1430237. doi:10.3389/or.2024.1430237
23. Jin L, Zhou Y, Han L, Piao J. MicroRNA302-367-PI3K-PTEN-AKT-mTORC1 pathway promotes the development of cardiac hypertrophy through controlling autophagy. *Vitro Cell Dev Biol Anim*. 2020;56(2):112–119. doi:10.1007/s11626-019-00417-5
24. Zhou G, Wu H, Yang J, et al. Liraglutide attenuates myocardial ischemia/reperfusion injury through the inhibition of necroptosis by activating GLP-1R/PI3K/Akt pathway. *Cardiovasc Toxicol*. 2023;23(3–4):161–175. doi:10.1007/s12012-023-09789-3
25. Zhao X, Yang F, Wu H, et al. Zhilong Huoxue Tongyu capsule improves myocardial ischemia/reperfusion injury via the PI3K/AKT/Nrf2 axis. *PLoS One*. 2024;19(4):e0302650. doi:10.1371/journal.pone.0302650
26. Chen W, Zhang Y, Wang Z, et al. Dapagliflozin alleviates myocardial ischemia/reperfusion injury by reducing ferroptosis via MAPK signaling inhibition. *Front Pharmacol*. 2023;14:1078205. doi:10.3389/fphar.2023.1078205
27. Zhang J, Yu P, Hua F, et al. Sevoflurane postconditioning reduces myocardial ischemia reperfusion injury-induced necroptosis by up-regulation of OGT-mediated O-GlcNAcylated RIPK3. *Aging*. 2020;12(24):25452–25468. doi:10.18632/aging.104146
28. Zhang XY, Huang Z, Li QJ, et al. Ischemic postconditioning attenuates the inflammatory response in ischemia/reperfusion myocardium by upregulating miR-499 and inhibiting TLR2 activation. *Mol Med Rep*. 2020;22(1):209–218. doi:10.3892/mmr.2020.11104
29. Song S, Wang Y, Wang HY, Guo LL. Role of sevoflurane in myocardial ischemia-reperfusion injury via the ubiquitin-specific protease 22/lysine-specific demethylase 3A axis. *Bioengineered*. 2022;13(5):13366–13383. doi:10.1080/21655979.2022.2062535
30. Xu G, Ma Y, Jin J, Wang X. Activation of AMPK/p38/Nrf2 is involved in resveratrol alleviating myocardial ischemia-reperfusion injury in diabetic rats as an endogenous antioxidant stress feedback. *Ann Transl Med*. 2022;10(16):890. doi:10.21037/atm-22-3789
31. Boyanpally A, Cutting S, Furie K. Acute ischemic stroke associated with myocardial infarction: challenges and management. *Semin Neurol*. 2021;41(4):331–339. doi:10.1055/s-0041-1726333
32. Schafer A, Konig T, Bauersachs J, Akin M. Novel therapeutic strategies to reduce reperfusion injury after acute myocardial infarction. *Curr Probl Cardiol*. 2022;47(12):101398. doi:10.1016/j.cpcardiol.2022.101398
33. Ryu KH, Hwang SH, Shim JG, et al. Comparison of vasodilatory properties between desflurane and sevoflurane using perfusion index: a randomised controlled trial. *Br J Anaesth*. 2020;125(6):935–942. doi:10.1016/j.bja.2020.07.050
34. Zhou T, Guo S, Wang S, Li Q, Zhang M. Protective effect of sevoflurane on myocardial ischemia-reperfusion injury in rat hearts and its impact on HIF-1alpha and caspase-3 expression. *Exp Ther Med*. 2017;14(5):4307–4311. doi:10.3892/etm.2017.5078
35. Xue Q, Yang D, Zhang J, et al. USP7, negatively regulated by miR-409-5p, aggravates hypoxia-induced cardiomyocyte injury. *APMIS*. 2021;129(3):152–162. doi:10.1111/apm.13100
36. Yang L, He K, Yao S, Zhang Y, Shen J.Sevoflurane inhibits neuroblastoma cell proliferation and invasion and induces apoptosis by miR-144-3p/YAP1 axis. *Basic Clin Pharmacol Toxicol*. 2021;129(4):297–307. doi:10.1111/bcpt.13629
37. Wu J, Cai W, Du R, et al. Sevoflurane alleviates myocardial ischemia reperfusion injury by inhibiting P2X7-NLRP3 mediated pyroptosis. *Front Mol Biosci*. 2021;8:768594. doi:10.3389/fmolb.2021.768594
38. Ao J, Zhang X, Zhu D. Sevoflurane affects myocardial autophagy levels after myocardial ischemia reperfusion Injury via the microRNA-542-3p/ADAM9 axis. *Cardiovasc Toxicol*. 2024;24(11):1226–1235. doi:10.1007/s12012-024-09908-8
39. Li Y, Xing N, Yuan J, Yang J. Sevoflurane attenuates cardiomyocyte apoptosis by mediating the miR-219a/AIM2/TLR4/MyD88 axis in myocardial ischemia/reperfusion injury in mice. *Cell Cycle*. 2020;19(13):1665–1676. doi:10.1080/15384101.2020.1765512
40. Lv H, Yu J, Qian X, et al. USP7 upregulated by TGF-beta1 promotes ferroptosis via inhibiting LATS1-YAP axis in sepsis-induced acute lung injury. *iScience*. 2024;27(6):109667. doi:10.1016/j.isci.2024.109667
41. Mori K, Iijima N, Higo S, et al. Epigenetic suppression of mouse Per2 expression in the suprachiasmatic nucleus by the inhalational anesthetic, sevoflurane. *PLoS One*. 2014;9(1):e87319. doi:10.1371/journal.pone.0087319
42. Hou Q, Yuan J, Li S, et al. Autophagic degradation of DHCR7 activates AKT3 and promotes sevoflurane-induced hippocampal neuroinflammation in neonatal mice. *Free Radic Biol Med*. 2024;222:304–316. doi:10.1016/j.freeradbiomed.2024.06.012
43. He W, Duan L, Zhang L. LOXL1-AS1 aggravates myocardial ischemia/reperfusion injury through the miR-761/PTEN axis. *Korean Circ J*. 2023;53(6):387–403. doi:10.4070/kcj.2022.0301
44. Liu W, Yan B, Yu H, et al. OTUD1 stabilizes PTEN to inhibit the PI3K/AKT and TNF-alpha/NF-kappaB signaling pathways and sensitize ccRCC to TKIs. *Int J Biol Sci*. 2022;18(4):1401–1414. doi:10.7150/ijbs.68980
45. Deng R, Guo Y, Li L, et al. BAP1 suppresses prostate cancer progression by deubiquitinating and stabilizing PTEN. *Mol Oncol*. 2021;15(1):279–298. doi:10.1002/1878-0261.12844
46. Gong M, Li Z, Zhang X, et al. PTEN mediates serum deprivation-induced cytotoxicity in H9c2 cells via the PI3K/AKT signaling pathway. *Toxicol In Vitro*. 2021;73:105131. doi:10.1016/j.tiv.2021.105131
47. Xiong W, Hua J, Liu Z, et al. PTEN induced putative kinase 1 (PINK1) alleviates angiotensin II-induced cardiac injury by ameliorating mitochondrial dysfunction. *Int J Cardiol*. 2018;266:198–205. doi:10.1016/j.ijcard.2018.03.054
48. Li Y, Cao Y, Xiao J, et al. Inhibitor of apoptosis-stimulating protein of p53 inhibits ferroptosis and alleviates intestinal ischemia/reperfusion-induced acute lung injury. *Cell Death Differ*. 2020;27(9):2635–2650. doi:10.1038/s41418-020-0528-x